# MICROSEISMIC SIGNATURES OF HYDRAULIC FRACTURE PROPAGATION IN SEDIMENT FORMATIONS

T. Fischer[(1)], S. Hainzl[(2)], Z. Jechumtalova[(1)], L. Eisner[(3)]
(1) Institute of Geophysics, Acad. Sci., Prague, Czech Republic
(2) GeoForschungsZentrum Potsdam, Germany
(3) *formerly* Schlumberger Cambridge Research, Cambridge, UK
e-mail: tomfis@ig.cas.cz

## ABSTRACT

Hydraulic fracturing is a common tool to increase the productivity of hydrocarbon reservoirs, which suffer of decreasing hydrocarbon pressure and permeability of gas/oil-bearing sediments. We analyzed a microseismic data set from hydraulic fracture stimulation of the gas field in West Texas. The data were recorded by an array of 8 three-component geophones deployed in a nearby vertical borehole. We used an automated wave-picking algorithm and obtained a high-density image of induced microearthquakes accompanying the hydraulic fracture growth. The event locations delineated a planar fracture growing predominantly in the horizontal direction; the vertical growth was limited by shale layers. The eastern and western wings of the fracture reached the lengths of 200 and 100 m, indicating an asymmetric fracture growth with 80% of the events located east from the injection. We find that the length of the hydraulic fracture increased, for different depth intervals, both linear and nonlinear in time. We use hydraulic fracture models to explain the spreading of the microseismic front, whose nonlinear time dependence could indicate either a diffusive fluid flow or a two-dimensional growth of the hydraulic fracture. By the maximum-likelihood fitting of the observed fracture growth and by inverting for its parameters, we find that the fracture was 7-10 mm wide and that nearly the whole injected volume was used for creating the new fracture, that is a negligible diffusive infiltration of the injected fluid into the reservoir rock occurred. We performed a limited moment tensor inversion to find the type of focal mechanism of the events accompanying the fracture growth. We show that a non-shear component is necessary to explain the observed seismograms which indicates that the micro-earthquakes are accompanied by some volumetric changes.

## INTRODUCTION

Canyon sandstone formation of West Texas contains significant resources of the tight gas, however, the existing reservoirs require stimulation by hydraulic fracturing to be produced economically. Due to a complex geological history and low permeability of the Canyon sandstones in this region (Marin et al., 1993) the hydraulic fracture stimulations are complex and frequently monitored for induced seismicity (Cipolla et al., 2005).

We have analyzed one hydraulic fracture treatment that was carried out in a nearly vertical borehole at depth intervals between 1604 and 1817 m. The map view of the treatment and monitoring wells is shown in Fig. 1 along with the initial locations of the largest events in the third stage of this treatment. Six injection stages lasting about 30 minutes each were utilized to stimulate the six depth intervals ranging between 10 to 34 m in length. The well casing in these intervals was perforated and sealed off by packers from previously perforated intervals (starting from the deepest depth interval). In order to decrease fluid loss the viscosity of the injected brine was increased by adding low concentration of polymer and $CO_2$. In the beginning of each stage, the injection rate was increased stepwise up to 100 l/s to result in a final wellhead pressure between 25 and 30 MPa. After more than 10 minutes of injection, proppant of grain size 0.6 mm was added to the fracturing fluid. The proppant concentration was gradually increased up to the final 1 kg/l. In each stage, more than 100 $m^3$ of fracturing fluid and about 20 $m^3$ of sand was placed into the reservoir formation.

The nearly vertical monitoring borehole was situated approximately 250 m from the treatment borehole. A vertical array of eight 3-component geophones was placed in the depth interval 1604 to 1817 m with a 30 m spacing. The geophones were oriented from the particle motion of P-waves generated by the perforation shots at the treatment well. However, due to the lack of the top part of the deviation survey of the treatment well, the relative position of treatment and monitoring wells is uncertain and also the resulting absolute orientation of the geophones as well as the absolute positions of the located microseismic events are uncertain (Bulant et al., 2006).

In this study we show results of advanced analyses of the four stages of the hydraulic fracture stimulation in
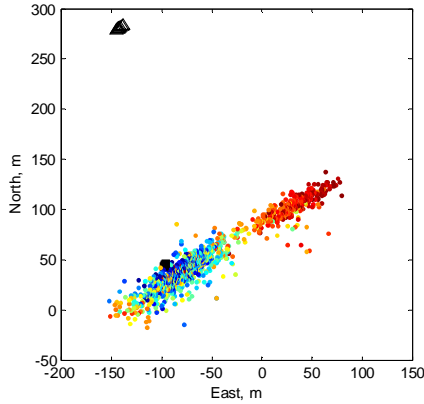
*Figure 1. Mapview of the hydraulic fracture geometry: Receivers are represented by black upside-down triangles at 280 m north, Perforations are represented by black squares approx -100 m east and 40 m north. Located microseismic events are represented by color-coded dots (colder colors correspond to earlier events).*

this formation. We show that the hydraulic fracture has approximately two-dimensional geometry which reduces to one-dimensional in the presence of sufficiently tough confining shale layers. For different injection stages and depth intervals we observe a different type (linear and nonlinear) of increase of the fracture length with time during the injection period. By numerical modeling of the observed fracture growth using the Carter′s (1957) model of hydraulic fracture, we obtain the geometry of the fracture and its growth speed. We also determine the moment tensors of selected events to find the possible contribution of non-shear components in focal mechanisms.

**LOCATION TECHNIQUE**

Due to the large amount of data, we use a fully automatic procedure (Fischer, et al. 2007) to resolve the hypocenter positions of induced events. Because of the vertical geometry of the receiver array, the *P*- and *S*-wave arrival times control only the hypocentral distance and depth, whereas the lateral position of the events along the fracture is constrained by the backazimuth. Hence, we measure both arrival times and polarizations of seismic waves. To obtain the maximum available number of induced events, we process the original continuous seismic data recordings to pick the *P*– and *S*– arrival times and polarizations. In this data set all observed *S*–wave amplitudes are larger than *P*–wave amplitudes and thus provide a much larger number of polarization measurements of sufficient quality than with *P*–waves.

Accordingly, we use a newly developed technique to determine the source backazimuth from *S*-wave waveforms. With this technique we determine the slowness vector of *S*-waves detected in a vertical array of receivers in smoothly varying isotropic medium (Eisner and Fischer, 2008). The slowness vectors determine backazimuth to the source which allows location of microseismic events using only shear waves in a single linear array of receivers. This technique was tested on both synthetic and real datasets showing significant improvements in backazimuth determination (i.e., locations). Fig. 2 shows cross-section through locations obtained by iterative search for hypocenter position $(x,y,z,t_0)$ at which the combination of the time residual and the azimuth residual is minimized (Fischer et al., 2008).
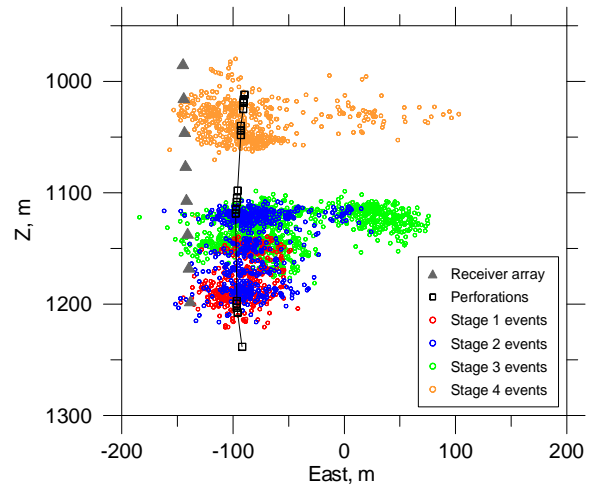


*Figure 2. Cross-section through preliminary locations of events detected during the first three stages of the hydraulic fracture stimulation.*

Fig. 2 illustrates that stages 1, 2 and 3 grew out-of-zone and stages 2 and 3 refractured previously stimulated parts of the reservoir. Such problem is also known as out-of-zone or out-of-pay growth in multi-stage fracturing and we shall call it a cross-stage fracturing in this article. Independent of localizing the microseismic events, the cross-stage fracturing can be detected by automated identification of multiplets, i.e. microseismic events with similar source mechanisms and nearly identical locations, which show mutually similar waveforms. We identified waveform similarity by analyzing the waveform cross-correlation. Fig. 3 shows cross-correlation matrix where red areas indicate cross-stage fracturing (Eisner, et al. 2006). The cross-stage fracturing was detected a few minutes after detecting the first microseismic events. The computation cost of this identification of cross-stage fracturing is a fraction of a second per detected microseismic event, thus making this application suitable for real-time monitoring. The identification of the multiplets

provides additional information to the locations of microseismic events and can be used to verify or justify the changes during hydraulic fracturing treatment. The early detection of the cross-stage fracturing could lead to real-time adjustments of the hydraulic fracturing.
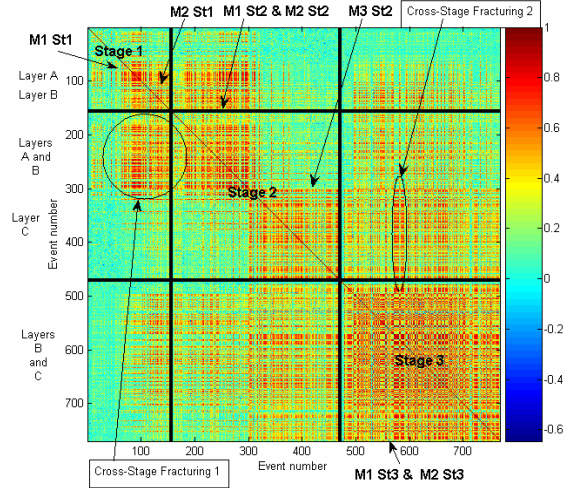


*Figure 3. Cross-correlation coefficients of all recorded waveforms between each pair of events detected during the first, second and third stage. The colour-bar on the right side of the plot represents cross-correlation coefficient. Events 1-157 were recorded during the first stage, events 158-471 were recorded during the second stage and events 472-769 were recorded during the third stage. Cross-stage fracturing 1 and 2 show examples of highly correlated events between the first and second stages and the second and third stages, respectively.*

To quantify the geometry of the microseismicity, we have carried out a principal component analysis of the hypocenter clouds illustrated in Fig. 4 for Stage 3. It shows that for all stages of this hydraulic fracturing treatment the induced seismicity is confined to a single plane of the hypocenter cloud. It also shows that stages 1 and 2 grew vertically as well as horizontally indicating out-of-zone fracturing (Eisner, et al. 2006). On the other hand, stages 3 and 4 show prevailing one-dimensional, subhorizontal growth.

To overcome the problem of weak P-wave amplitudes, we carried out a constrained two-dimensional localization that requires only S-wave picks; we use also P-wave picks where available. Our approach is based on the premise that all the hypocenters accompanying the hydrofracture growth lie on a vertical plane that is defined by the strike of the hypocenter cloud (see Fig. 1). Then the lateral position of the hypocenters is determined by the intersection of two vertical planes: the plane of the hydraulic fracture and the plane defined by the S-
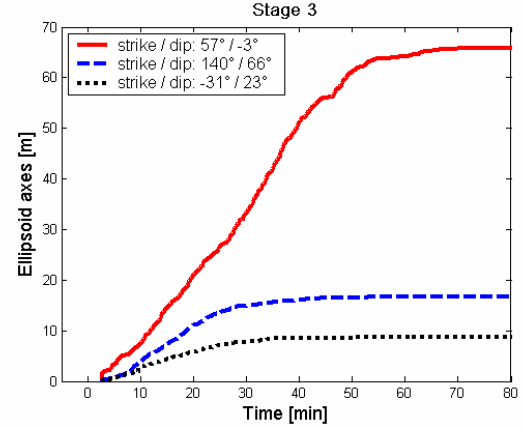


*Figure 4. Time dependence of the main axes of the ellipsoidal envelope determined by principal component analysis of the hypocenter clouds for stage 3. Zero time corresponds to the onset of injection.*

wave backazimuth. The hypocenter depth is constrained by the moveout of P- or S-wave arrivals along the vertical array. Consequently, the location problem reduces to a two-dimensional one, with the depth and the coordinate along the strike of the hydrofracture as unknowns and with S-wave arrival times and backazimuths as data. We applied the modified localization scheme to the data and obtained hypocenter locations of more than 10,500 microearthquakes, which is about four times more than that when using the full three-dimensional (3D) localization. The increase accounts not only for the events with weak P-wave amplitudes, but also for the fact that S-waves have, in general, a larger signal-to-noise ratio than P-waves. Fig. 5 shows a cross-section of the hypocenter locations resulting from this location technique.

Fig. 5 shows several important differences from Fig. 2 derived with traditional locations based on both *P*- and *S*-waves. Note, that the seismicity gap at the eastern wing (between -30 and 0 m in Fig. 3) of the hydraulic fracture is not present in Fig. 5. Detailed analyses reveals that *P*-waves detected east of this seismic gap have opposite polarity than *P*-waves detected west of the seismic gap. This implies that there is a *P*-wave nodal line, i.e. *P*-waves from events located in the seismic gap of Fig. 2 have zero energy radiated towards the vertical receiver array. Such seismic gaps are frequently interpreted as "stress shadow effects" (Fisher, et al., 2004), however as illustrated in this study they can be artifact of receiver geometry and radiation pattern. Additional benefit of locating the weaker events shows for fracture growth of the first stage - from locations in Fig. 5 we can see continuous growth of the microseismic cloud from the vicinity of the lowest perforations (used for the first stage) to the upper layers resulting in larger fracture size than

3

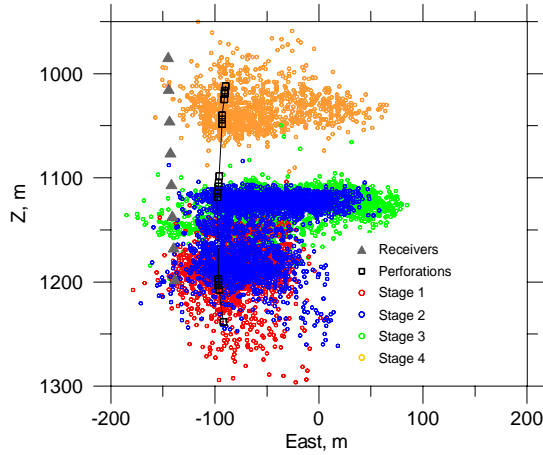estimated from locations of the strongest events (Fig. 2).



*Figure 5 Cross-section through locations of events detected during the first three stages of the hydraulic fracture stimulation. The locations were constrained to be in a vertical plane defined by the fracture azimuth shown in Fig. 1*

## FRACTURE GROWTH

Reducing the hypocetal locations to two dimensions, we can use two representations, horizontal elongation versus time (*X-t*-plots) and depth versus time (*Z-t*-plots), to examine the temporal growth of the microseismic cloud as shown in Fig. 6. The injection point can be easily identified as the position of the earliest occurring events. The rate and the character of microseismicity spreading are clearly visible both in the horizontal and depth views and are comparable with the injection regime. Here we shall point out several characteristics of the space-time plots. In contrast to the depth view, the horizontal-view plots show continuous growth of the hydraulic fracture. Due to the limited height of sediment horizons, the growth in each horizon may be viewed as a one-dimensional one. It is apparent that the stages differ in the characteristics of the horizontal growth. Whereas the seismicity at stages 1 and 3 started in a narrow range of *X* coordinates, stages 2 and 4 show a smeared picture with the first events occurring within the range of more than ±20 ft from the injection. The microseismicity at the deepest stage 1 was further delayed by 10 minutes after the start of the injection compared to only less than 3 minutes at the later stages. A striking feature distinguishing the stages is the shape of the envelope of the *X* coordinates: whereas the stages 1 and 2 display a nonlinear spreading of the maximum *X*-coordinate, the

seismicity at later stages shows a pronounced linear growth. To our best knowledge this is so far the most convincing observation of a linear growth of a triggering front. In most injection experiments carried out in granite, a square-root type of spreading was observed, which has been attributed to a diffusion process of the fluid in the host rock. Besides the hydraulic diffusion, the nonlinear shape of the envelope of *X* coordinates could be attributed to a 2-D growth of microseismicity. We have evaluated (Fischer et al., 2008) the contribution of these two processes by modeling of the hydraulic fracture growth and shown that the diffusion process is negligible. The asymmetry of the microseismic cloud visible in Fig. 2 and 5 becomes even more pronounced in the *X-t* plot in Fig. 6. Note that the asymmetry is displayed not only in the much larger length of the eastern wing, but also in the larger speed of growth to the east than to the west; see stages 2, 3, and 4, indicating that stress barrier does not stop the horizontal propagation of the western wings of the induced fractures. At these stages, the asymmetry manifests itself also in the discontinued duration of the activity after injection shut-in that occurs only at the eastern wing.
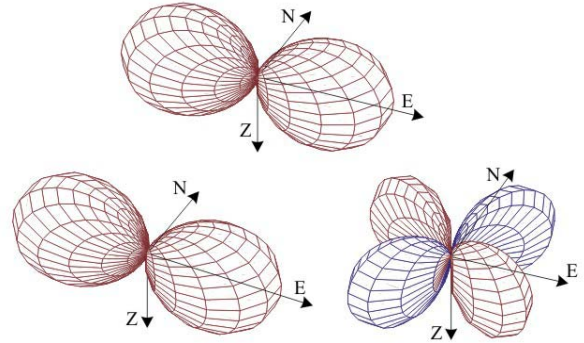


*Fig. 7 — Test of source mechanism inversion in a single vertical borehole, red, resp. blue, colour represents positive, resp. negative, radiation of direct P-waves. Upper plot represents radiation patern of crack opening in the east-west direction – the input model. Lower left plot represents inversion result with the closest source mechanism to the input data. Lower right represents another inversion result representing pure shear source. Both inverted solutions shown in lower plots fit all seismic data with exactly the same misfit.*
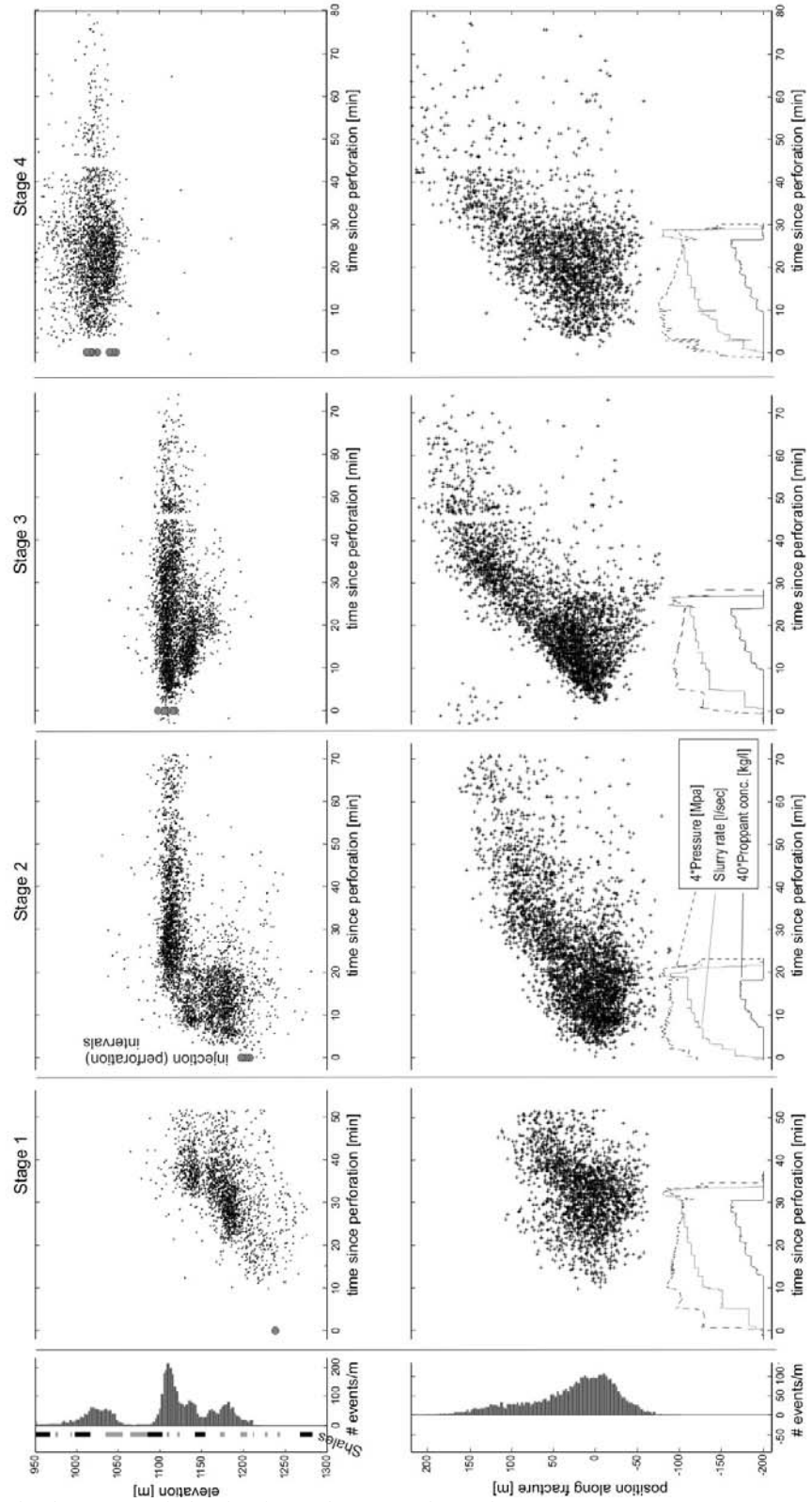
*Figure 6. Time dependence of the hypocentral depth, (left), distance along the fracture extension (center), and injection regime (right). The injection points are indicated by grey ovals. The distribution of event depth and position along the fracture is shown at bottom.*

## MECHANISMS OF THE INDUCED EVENTS

Finally, we have applied a new method to invert source mechanisms of seismic events observed from a single (near vertical) array of receivers (Jechumtálová and Eisner, 2007). First we tested this method on synthetic datasets. We show that crack-opening seismic event recorded on a single vertical array can incorrectly be inverted as a pure-shear seismic event. Fig. 7 shows results of source mechanism inversion in a single vertical borehole. We tested inversion of synthetic dataset of crack opening in the east-west direction. Our test showed that inverting such data from a single borehole can result in nearly arbitrary orientation of the shear part of the source. In this case the best fitting shear source mechanism is the pure shear strike-slip faulting with fault plane not related to the crack opening at all as shown in lower right plot of Fig. 7. This test shows that if the induced events have partially non-shear source mechanisms the best fitting shear mechanism is not representative of any crack orientation as thought earlier (Sorrels and Warpinski, 1999).
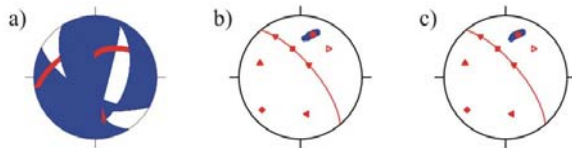


*Fig. 8 ─ Study of source mechanism of a selected event from Stage 2: a) all fault planes of shear source satisfying observed seismic data; b) Jordan-Riesdel representation of uncertainty due to seismic noise; c) Jordan-Riesdel representation of uncertainty due to uncertainty in the location.*

We have applied this technique to twelve representative events from stage 2 of this dataset. We found that the eleven of the twelve selected events have source mechanisms requiring some non-shear component, i.e. eleven of the twelve events are inconsistent with pure shear faulting. Fig. 8 illustrates an example for one of the selected events. The plot 8a) reveals uncertainty in orientation of the shear source. For study of the sensitivity to the seismic noise and location uncertainty the plots 8b) and 8c) show the mechanisms with maximum shear source consistent with the observed data and its uncertainty. The blue dots in 8b) and 8c) represent all possible source mechanism within the uncertainty due the noise and location error. The red square if 8b) and 8c) represents the position of a corresponding pure shear mechanism. None of the red dots coincides with the red square indicating that the source mechanism is not consistent with pure shear source. Thus source mechanism must be partly non-shear even when seismic noise and location uncertainty are considered.

This also implies that inversion for pure shear mechanisms of the induced events (in this dataset) provides misleading information. The non-shear nature of the source mechanisms is also consistent with the nearly zero leak-off and very narrow band of seismicity indicating that the induced events are directly colocated at the newly created hydraulic fracture.

## CONCLUSIONS

New insights into the physics of hydraulic fracturing were gained by the developed techniques for processing of the seismic dataset acquired during hydraulic fracture monitoring. The advanced locations based on the *S*-wave backazimuth revealed continuous growth of the hydraulic fracture through apparent gap. This gap was caused by the monitoring array geometry and *P*-wave radiation pattern, not a stress shadow as previously thought. Furthermore, these locations reveal longer and higher fracture geometry, indicating that hydraulic fracture grew vertically connecting several sand layers overcoming shale barriers. This vertical growth out-of-zone was confirmed by multiplet analyses indicating that the lower three treatments stimulated the same part of the reservoir and could be combined into a single fracturing stimulation. Fracture grew nearly linearly in the horizontal directions with asymmetric speeds of approximately 16 ft/min to east and 8 ft/min to west. This observation implies that the fracture asymmetry is not caused by a hydraulic fracture barrier on the western wing. A limited analyses of the source mechanisms of the induced seismic events provide evidence that these events are directly located at the hydraulic fracture and most probably they are not shear failures on pre-existing natural faults. Thus the best fitting shear mechanism does not provide any information about the natural fracture orientation

## ACKNOWLEDGMENTS

## REFERENCES

Bulant, P., Eisner, L., Pšenčík, I. and Calvez L.H.J. (2006). "Borehole Deviation Surveys Are Necessary For Hydraulic Fracture Monitoring." Paper SPE 102788 presented at the SPE Annual Technical Conference and Exhibition, San Antonio, Texas, USA, 24-27 September.

Cipolla, C., Peterman, F., Creegan, T., McCarley, D. and Nevels H., (2005). "Effect of well placement on production and frac design in a mature tight gas field". Paper SPE 95337 presented at the SPE

Annual Technical Conference and Exhibition, Dallas, Texas, USA.9-12 October.

Eisner L., and Fischer, T. (2008). "Determination of S-wave polarization from a linear array of receivers". *Geoph. J. Int*., submitted.

Eisner, L., Fischer, T. and Calvez L.H.J. (2006). "Detection of repeated hydraulic fracturing (out-of-zone growth) by microseismic monitoring", *The Leading Edge* **25**, (5): 547–554.

Fischer, F., Boušková, A., Eisner, L., Calvez, L.H.J. (2007). "Automated P- and S-wave picking of microearthquakes recorded by a vertical array." 69th Meeting, EAGE, Expanded Abstracts P217.

Fischer, T., Hainzl, S., Eisner, L., Shapiro S.A. and Calvez L.H.J. (2008). "Microseismic signatures of hydraulic fracture growth in sediment formations: Observations and modeling", *J. Geophys. Res.*, in print..

Fisher, M.K., Heinze, J.R., Harris, C.D., Davidson, B.M., C.A. Wright, K.P. Dunn., (2004). "Optimizing horizontal completion techniques in the Barnett shale using microseismic fracture mapping". Paper SPE 90051 presented at the SPE Annual Technical Conference and Exhibition, Houston, Texas, USA, 26 - 29 September.

Jechumtalova, Z. and Eisner, L. (2007). "Non-double-couple seismic events induced by hydraulic fracturing", in preparation.

Marin, B.A., Clift, S.J., Hamlin, H.S. and Laubach S.E. (1993). "Natural fractures in Sonora Canyon sandstones, Sonora and Sawyer Fields, Sutton County, Texas". Paper SPE 25895 presented at the SPE Rocky Mountain regional low permeability reservoir symposium held in Denver, CO, USA,.12-14. April.

Rutledge, J.T. and Phillips, W.S. (2003). "Hydraulic stimulation of natural fractures as revealed by induced microearthquakes, Carthage Cotton Valley gas field, east Texas". *Geophysics*, **68**(2): 441-452.

Sorrels, G. and Warpinski, N.R. (1999). "System and method for determining the distribution and orientation of natural fractures", US patent No. 09/015,457.